

SCIENTIFIC REPORTS

**OPEN**

Ultrahigh Oxidation Resistance and High Electrical Conductivity in Copper-Silver Powder

Received: 09 September 2016
Accepted: 24 November 2016
Published: 22 December 2016

Jiaxiang Li¹, Yunping Li^{1,2}, Zhongchang Wang³, Huakang Bian⁴, Yuhang Hou⁴, Fenglin Wang⁴, Guofu Xu¹, Bin Liu² & Yong Liu²

The electrical conductivity of pure Cu powder is typically deteriorated at elevated temperatures due to the oxidation by forming non-conducting oxides on surface, while enhancing oxidation resistance via alloying is often accompanied by a drastic decline of electrical conductivity. Obtaining Cu powder with both a high electrical conductivity and a high oxidation resistance represents one of the key challenges in developing next-generation electrical transferring powder. Here, we fabricate a Cu-Ag powder with a continuous Ag network along grain boundaries of Cu particles and demonstrate that this new structure can inhibit the preferential oxidation in grain boundaries at elevated temperatures. As a result, the Cu-Ag powder displays considerably high electrical conductivity and high oxidation resistance up to approximately 300 °C, which are markedly higher than that of pure Cu powder. This study paves a new pathway for developing novel Cu powders with much enhanced electrical conductivity and oxidation resistance in service.

For electrical transferring powders applied in numerous areas such as electronic packaging, printed electronic devices and electromagnetic interference shielding^{1–5}, high electrical conductivity and good oxidation resistance together are often required. Despite that the pure metal powders such as Cu show high conductivity, they usually demonstrate extremely low oxidation resistance. After oxidation, the rapid coverage of non-conductive oxide scales on surface results in an insulating effect between Cu particles, which in turn deteriorates significantly electrical conductivity of Cu powder. On the other hand, Ag powders possess high oxidation resistance and high electrical conductivity, but they are expensive and exhibit the electro-migration phenomena at elevated temperatures, which obstruct their widespread applications^{6,7}.

Enhancing oxidation resistance whilst maintaining high electrical conductivity of Cu powder has been a subject of intensive research in the last decades because of both the fundamental scientific importance and the technological applications. However, improving oxidation resistance of Cu powder via alloying is generally accompanied by a dramatic decrease in electrical conductivity. For example, alloying Cu with Ti, Mg, Al, Pd, Ag, Nb or Cr can raise oxidation resistance of Cu by several orders of magnitude^{8,9}, but the electrical conductivity falls to 10–30% of pure Cu^{10,11}. This is attributed to the fact that the alloying elements tend to increase the scattering rate of conducting electrons at point defects, leading to the increase in electrical resistivity of the metal¹². Alternatively, coating Cu particle with Ag by chemical processes seems to represent a prospective way of promoting oxidation resistance without sacrificing the electrical conductivity^{13–15}. However, such enhancement turns out not to be striking due to the low adhesive force at the Cu-core/Ag-shell interface and also for the loose microstructures of Ag shells on Cu particles^{16,17} that are unable to obstruct the inward diffusion of O. For electrical transferring Cu powder, these two essential properties, high electrical conductivity and high oxidation resistance, seems always contradictory.

Oxidation of metals is sensitive to chemical composition and surface structure, and often occurs first from the crystalline defects such as grain boundaries (GBs) and dislocation sites owing to their high Gibbs free energy, and then spreads into the entire surface¹⁸. Therefore, the key to producing conducting yet high oxidation-resistant Cu powder is to seek an appropriate microstructure in which the initiation of oxidation at crystalline defects is effectively retarded while the scattering effect of conducting electrons in particles is minimized. It is well acknowledged

¹School of Materials Science and Engineering, Central South University, Changsha, China. ²State Key Lab for Powder Metallurgy, Central South University, Changsha, China. ³Advanced Institute for Materials Research, Tohoku University, 2-1-1 Katahira, Aoba-ku, Sendai 980-8577, Japan. ⁴Institute for Materials Research, Tohoku University, 2-1-1 Katahira, Sendai, Miyagi 980-8577, Japan. Correspondence and requests for materials should be addressed to Y.L. (email: lyping@csu.edu.cn) or B.L. (email: binliu@csu.edu.cn)

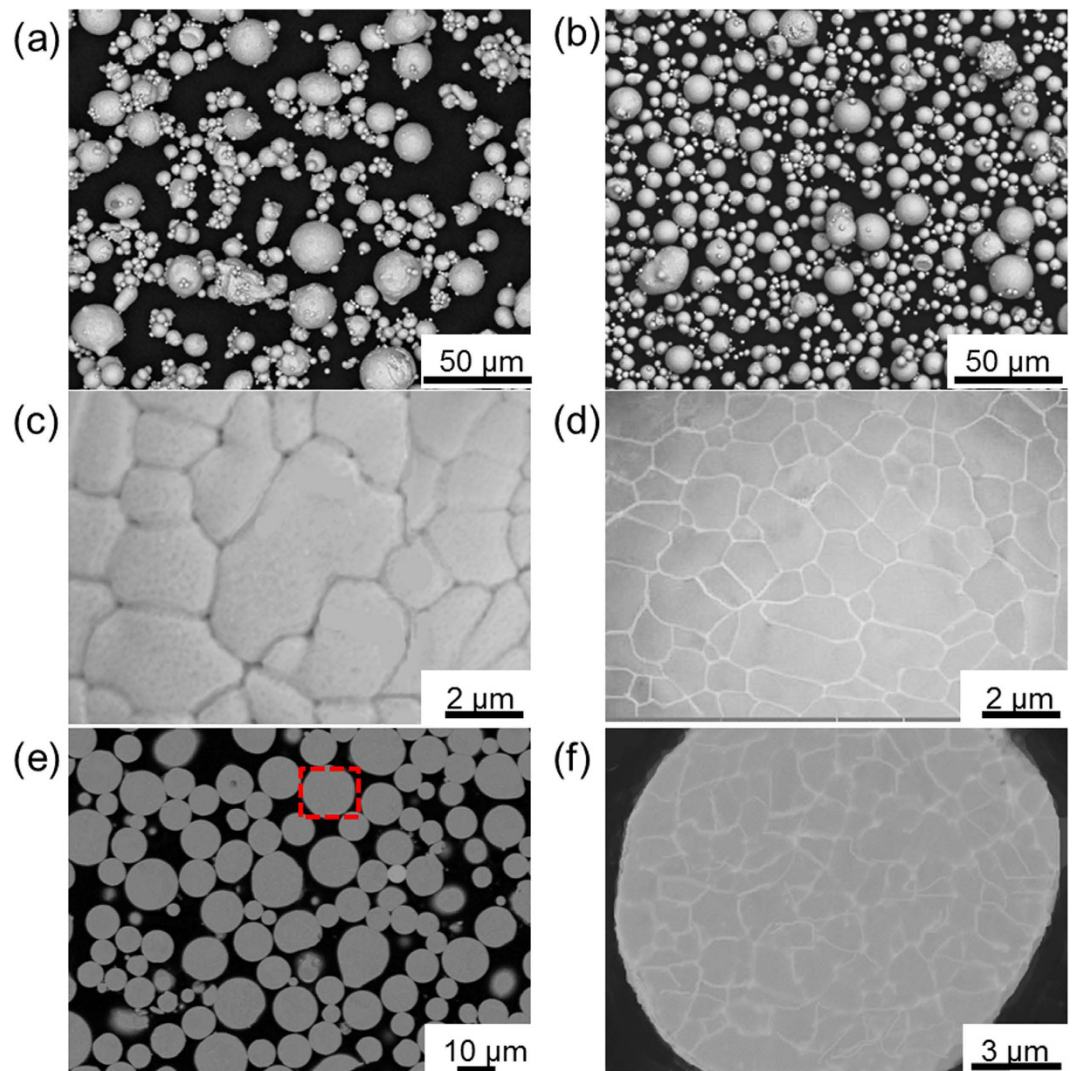


Figure 1. Microstructure of three Cu powders. (a,b) BEI images of the as-atomized pure Cu powder (a) and Cu-5Ag powder (b). (c,d) Enlarged BEI images highlighting the surface structure of the as-atomized Cu-Ag particle before (c) and after (d) aging at 250 °C for 60 min. (e,f) Cross-section view of the aged Cu-Ag powder (e) and the corresponding enlarged image (f).

that GBs can often serve as preferred sites for secondary phase precipitation because of their high interfacial energy possibly originated from the disordered arrangement of atoms and the higher proportion of lattice defects compared to matrix¹⁹. It is hence considered that only if the precipitates on these defects are chemically inert yet electrically conducting, the initiation of oxidation could be inhibited greatly. In this regard, if the particles are characterized by a high density of conducting and inert precipitates at GBs while the matrix is free of alloying elements, metal powders are expected to exhibit ultrahigh oxidation resistance without sacrificing electrical conductivity.

Cu-Ag alloy powder may be an ideal candidate to fulfill this hypothesis because Ag and Cu are utterly inter-dissolvable at high temperature, while at low temperature, most of Ag precipitates out from Cu preferentially along GBs²⁰. This will give rise to Cu particles featured by Ag network along the GBs, consequently purifying Cu matrix. Such Ag network along GBs is helpful to enhance the oxidation resistance via hindering preferential oxidation due to the intrinsic inert nature of Ag. On the other hand, due to the close lattice parameters of Ag and Cu, residual Ag in Cu matrix has been proven not to be detrimental to the electrical conductivity of Cu^{21–23}. Here, we fabricate such Cu-Ag powder with continuous Ag network distributed along GB of Cu particles and demonstrate that this new structure can inhibit the preferential oxidation at GB even at elevated temperature. As a result, Cu-Ag powder displays considerably high electrical conductivity and high oxidation resistance up to approximately 300 °C, markedly higher than pure Cu powder.

The composition of Cu-Ag alloy was determined by using Cu-Ag binary phase diagram²⁴. For Cu-5 wt% Ag alloy, Cu and Ag are completely soluble to each other at temperature higher than 600 °C, and at lower temperature Ag will precipitate from Cu matrix preferentially along the lattice defects such as BGs. Alloy with higher Ag concentration would give rise to much rougher surface after precipitation, which is harmful to the flowability of powder from our preliminary research.

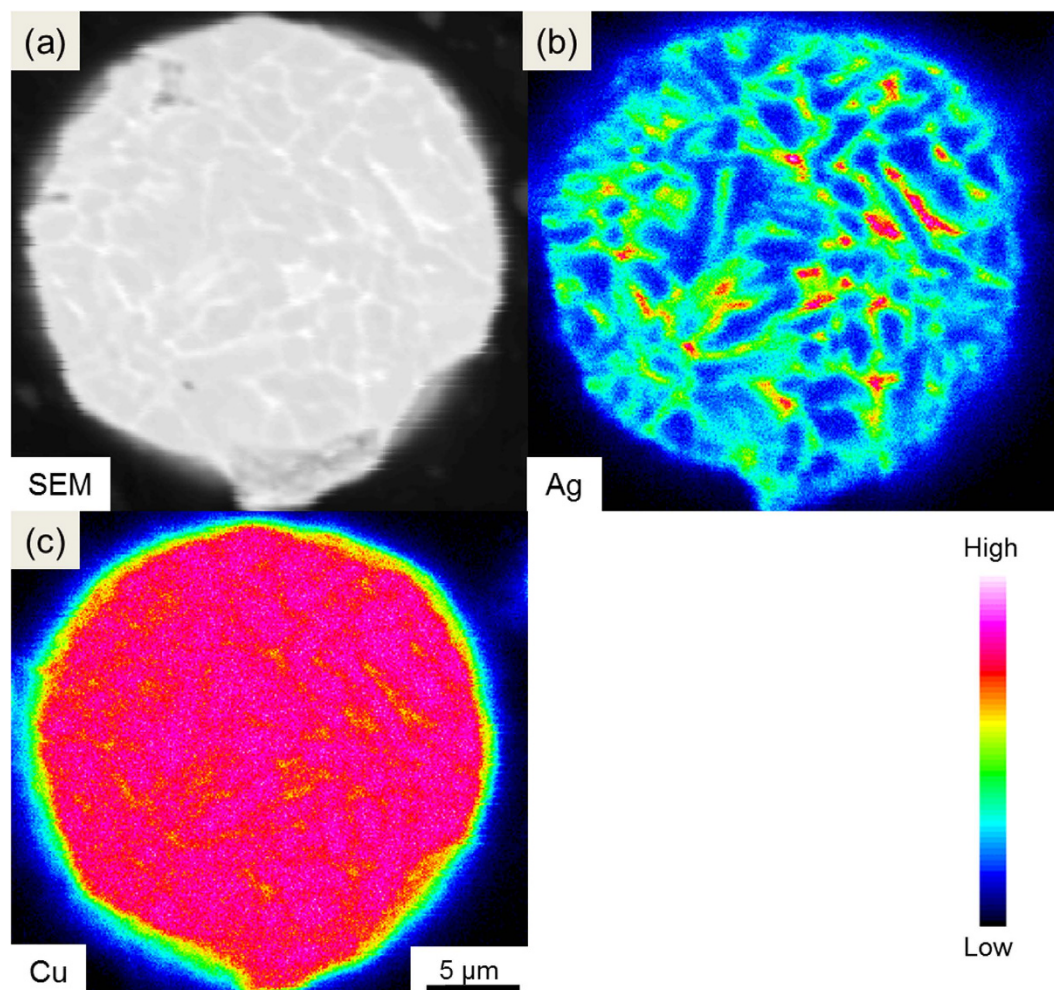


Figure 2. EPMA analysis. EPMA analysis of elemental distribution of Cu and Ag on the cross section of the Cu-Ag particle after aging at 250 °C for 60 min: (a) BEI image, (b) Ag, and (c) Cu.

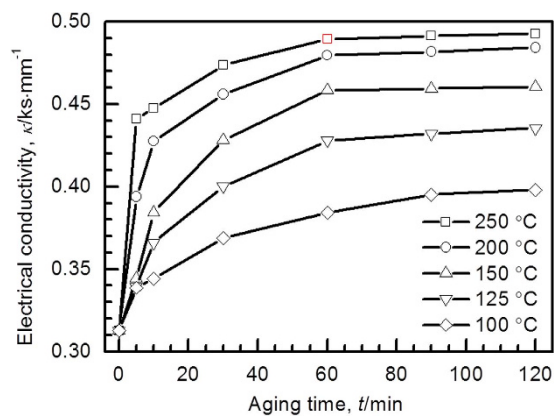


Figure 3. Aging time dependence of electrical conductivity. Electrical conductivity for Cu-Ag powder as a function of aging time up to 120 min. The aging temperature increases from 100 to 250 °C at an interval of 50 °C.

Results

Figure 1a,b shows the profiles of pure Cu and as-atomized Cu-Ag powders, both of which indicate that the microstructure is characterized by spherical particles with smooth surface. The GBs of the as-atomized Cu-Ag particles are visible and exhibit darker contrast in the BEI mode. After the aging treatment (250 °C, 1 h), the contrast of GBs turns bright, which suggests preferential precipitation of Ag along GBs (Fig. 1d), forming a continuous network.

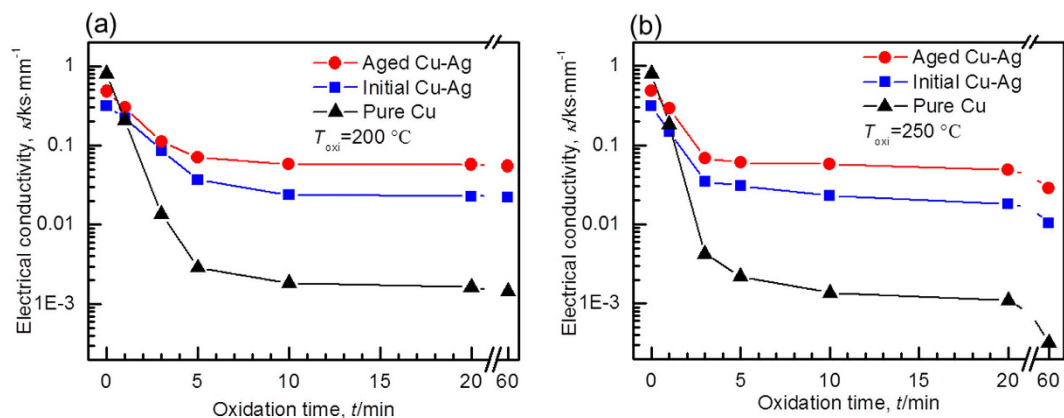


Figure 4. Electrical conductivity as a function of oxidation time. The change in the electrical conductivity during the oxidation process for the three types of Cu-based powders at (a) 200 °C and (b) 250 °C.

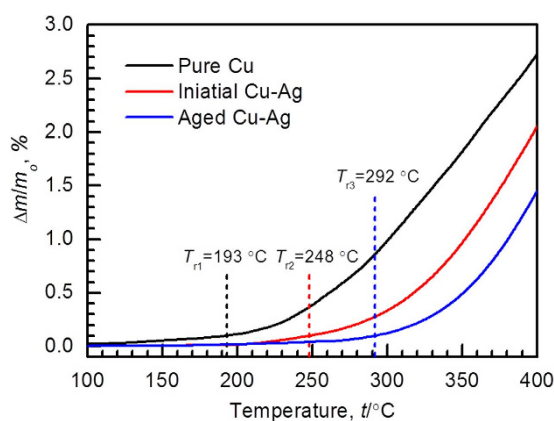


Figure 5. Thermogravimetric Analysis. Thermogravimetric curves of three Cu-based alloy powders. The heating rate is $30\text{ }^{\circ}\text{C}/\text{min}$. The starting points for the oxidation, denoted as T_{r1} , T_{r2} and T_{r3} , are assumed upon the specific mass gain (D_{m/m_0}) hitting 0.1%.

The cross-section view of the aging-treated Cu-Ag particles reveals that Ag atoms precipitate at GBs of the surface and the interior of particles, constituting a three-dimensional Ag network (Fig. 1e,f). Such distribution of Ag in the cross section of Cu particles can be observed more clearly by using EPMA elemental distribution (Fig. 2), in consistent with the Cu-Ag binary phase diagram. Although Cu and Ag are inter-dissolvable at high temperature, the solubility of Ag in Cu matrix decreases dramatically at lower temperature ($250\text{ }^{\circ}\text{C}$)^{25,26}, giving rise to the formation of continuous Ag network along GBs.

Figure 3 shows the electrical conductivity of Cu-Ag powder after aging at 100 to $250\text{ }^{\circ}\text{C}$. At each aging temperature, the electrical conductivity increases substantially before 40 min and then gradually reaches a constant value. For example, the electrical conductivity for the powder aged at $250\text{ }^{\circ}\text{C}$ for 60 min reaches a maximum value of about $0.49\text{ ks}\cdot\text{mm}^{-1}$, which is more than 50% higher than that of initial powder ($0.31\text{ ks}\cdot\text{mm}^{-1}$). For a given aging time, the electrical conductivity grows significantly with the aging temperature, while such tendency is not so obvious at the temperature above $200\text{ }^{\circ}\text{C}$ implying that further rise in aging temperature is not beneficial to the electrical conductivity.

Figure 4a,b shows the electrical conductivity as a function of oxidation time for the Cu, as-atomized Cu-Ag and aging-treated Cu-Ag ($250\text{ }^{\circ}\text{C}$, 1 h) powders. Although Cu powder displays the highest electrical conductivity in the beginning, its electrical conductivity falls sharply during oxidation in comparison to the other two powders. Note that at the two temperatures ($200\text{ }^{\circ}\text{C}$ and $250\text{ }^{\circ}\text{C}$), the aging-treated powder shows an extremely high electrical conductivity for a given exposure time, and its decreasing rate is the lowest among the three powders. For example, Cu powder at oxidation time of 0 min is as high as $0.78\text{ ks}\cdot\text{mm}^{-1}$, which is nearly 1.5 times and 2.5 times higher than that of the aging-treated and as-atomized Cu-Ag powders. However, once after oxidation at $200\text{ }^{\circ}\text{C}$ for 5 min, the electrical conductivity of Cu powder drops to as low as $2 \times 10^{-3}\text{ ks}\cdot\text{mm}^{-1}$, which is 1/40 and 1/20 of that of the aging-treated and as-atomized Cu-Ag powders subjected to the comparable extent of oxidation, respectively. These results indicate that the Cu-Ag powder after aging exhibit both high electrical conductivity and high oxidation resistance, which can be attributed to the formation of a continuous Ag network along GBs.

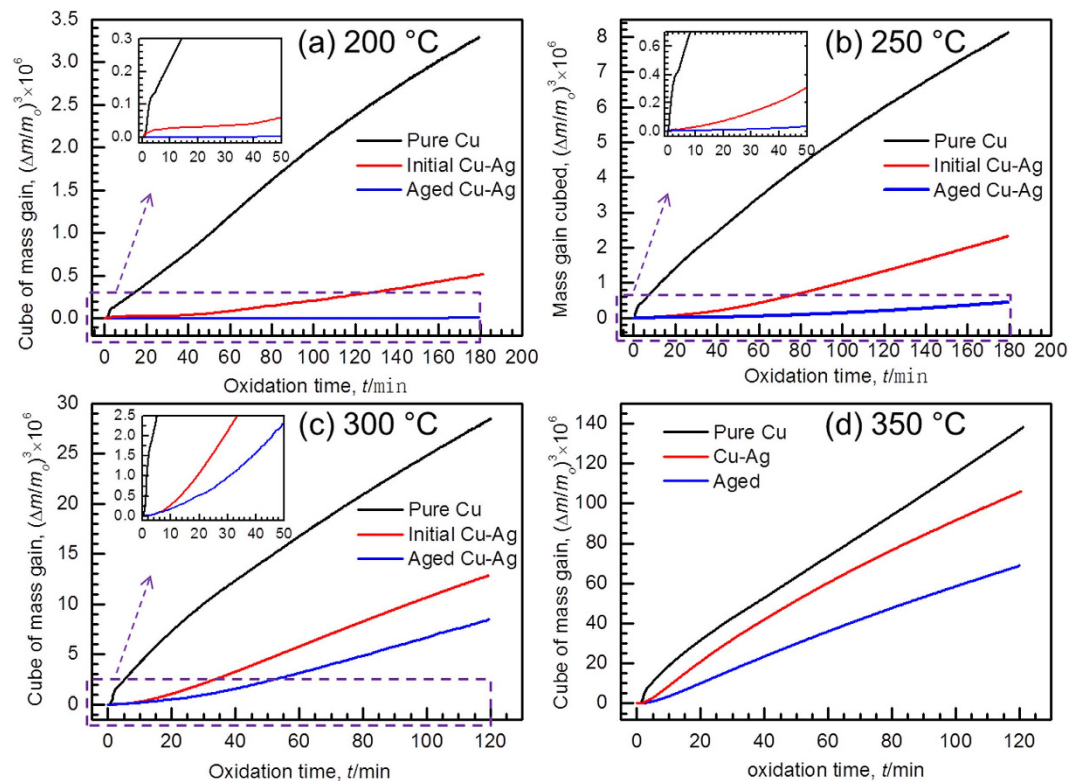


Figure 6. Oxidation isotherm. Oxidation isotherms for the three Cu-based powders at (a) 200 °C, (b) 250 °C, (c) 300 °C, and (d) 350 °C.

Figure 5 shows mass change ($\Delta m/m$) as a function of temperature obtained in flowing air at a heating rate of 30 °C/min, which the difference of oxidation behavior between the three powders can be seen clearly. The mass change of Cu powder varies insignificantly before 200 °C, yet goes up markedly with the increase of temperature. The same trend is observed for the as-atomized and aging-treated Cu-Ag powders, but their increase onset is higher for the aging-treated Cu-Ag than the as-atomized Cu-Ag. For a quantitative evaluation on the oxidation behavior, we choose the value of $\Delta m/m$ of 0.1% as the starting point of oxidation. The starting points of oxidation of pure Cu, as-atomized Cu-Ag, and aging-treated Cu-Ag powders are estimated to be 193, 248 and 292 °C, respectively, suggesting that the aging-treated Cu-Ag powder exhibits a much enhanced oxidation resistance in comparison to the as-atomized Cu-Ag and Cu powder by approximately 45 and 100 °C, respectively.

Figure 6 shows the mass change as a function of time for the three powders after oxidation at 200, 250, 300, and 350 °C. The oxidation rate for the two Cu-Ag powder samples is extraordinarily low in the beginning, while the mass change of Cu powder ascends much more substantially even at the very beginning (see the inserts in Fig. 6a–c). In contrast to the other two powders, the aging-treated Cu-Ag powder shows the highest oxidation resistance despite of the oxidation condition.

Figures 7, 8 and 9 show the typical BEI images for particle surface of the three powders after oxidation at 200 °C for different durations. In the case of Cu powder, the GBs, which are characterized by black dots (oxide), are observed to be readily affected by O even under oxidation for 0 min (Fig. 7a). The dots become larger and the number of dots increases significantly with the oxidation proceeding (b to c). After oxidation for longer than 5 min, GBs become ambiguous and the interior of grain matrix becomes rough, which is characterized by larger black dots inside the grains. This suggests that oxidation of pure Cu occurs preferentially at GBs and extends into matrix thereafter.

In the case of the as-atomized Cu-Ag powder, since no aging treatment is carried out prior to oxidation, GBs are free of Ag precipitates before oxidation. In the oxidation process, the contrast of some GBs turns bright, suggestive of precipitation of Ag on GBs during oxidation. There are no dark dots observed at GBs with Ag precipitates, implying its inhibiting effect on oxidation surrounding GBs. Conversely, some GBs are free of Ag and the area along these GBs is full of dark dots. This again implies preferential oxidation along Ag-free GBs. Further microstructure observation of sample surface of the aging-treated Cu-Ag powder after various oxidation periods reveals an extraordinary oxidation resistance, as shown in Fig. 9. Invariably, GBs are characterized by continuous uniform distribution of Ag (white contrast) throughout the oxidation. Even in the case of oxidation after 10 min, the Ag network is clearly apparent, although there are a few of dark dots inside the grains.

Figure 10 shows EDS spectra across typical GBs of the three powders, where the positions of GB are highlighted by blue dashed lines. For comparison, the relative intensity of each element is plotted in the same range. It can be clearly observed that overall intensity of O for the pure Cu particle increases significantly in the progress of oxidation. This is particularly evident at GBs where O peak intensity (corresponding valley for Cu intensity)

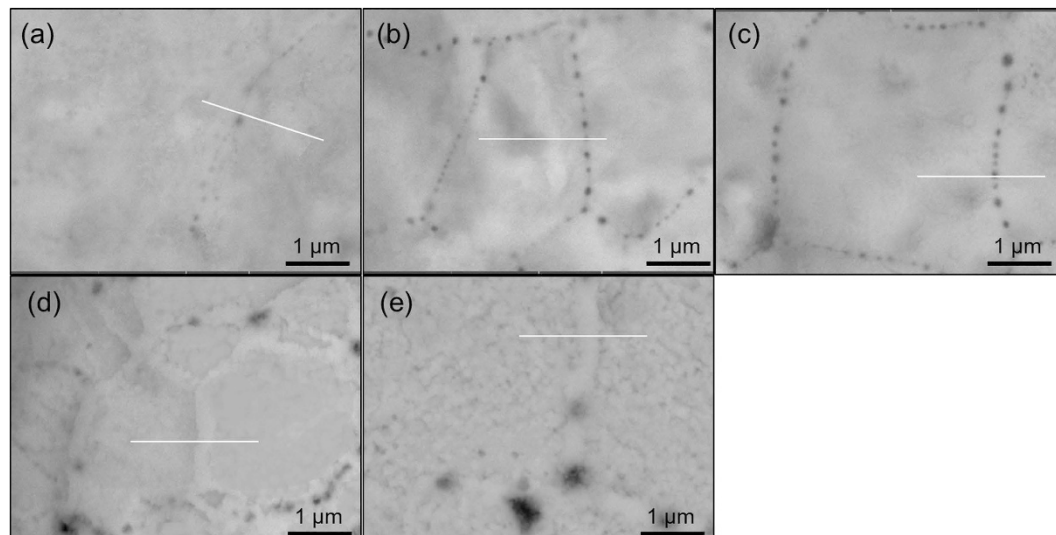


Figure 7. Structural evolution of the pure Cu. (a–e) Backscattered scanning electron images for the pure Cu powder after an oxidation period of 0 min (a), 1 min (b), 3 min (c), 5 min (d) and 10 min (e) at 200 °C.

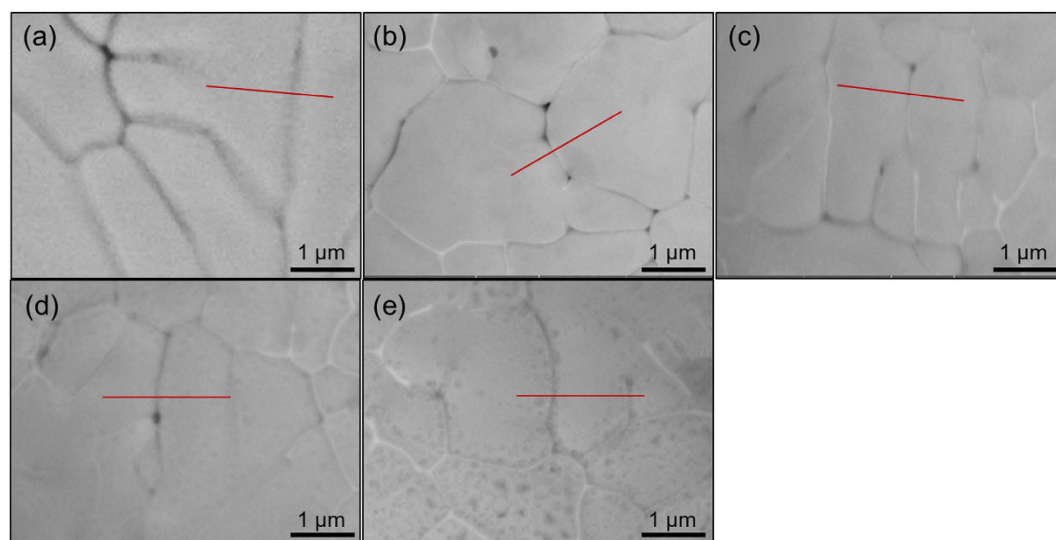


Figure 8. Structural evolution of the initial Cu-Ag powder. (a–e) Backscattered scanning electron images for the initial Cu-Ag powder after an oxidation period of 0 min (a), 1 min (b), 3 min (c), 5 min (d) and 10 min (e) at 200 °C.

is observed obviously and becomes much more pronounced with the oxidation proceeding. In contrast, for the as-atomized Cu-Ag, O peaks in both GBs and the interior of matrix are not so protruding (Fig. 10a), suggesting that oxidation resistance is improved by adding Ag. Some Ag peaks are observed along GBs. However, O intensity is relatively higher at GBs compared to the matrix implying that oxidation at GBs is not suppressed completely. For the aging-treated powder, strong Ag peaks together with O valleys at GBs are clearly observed throughout oxidation, suggesting strong inhibition of oxidation at GBs by Ag precipitation. In addition, in grain matrix, O intensity is a little smaller for the aging-treated Cu-Ag particles than the as-atomized Cu-Ag ones.

Discussion

It can be inferred from the aforementioned results that the addition of Ag into Cu and the subsequent aging treatment together contribute to high electrical conductivity and high oxidation resistance. This is attributable to the presence of the continuous Ag network along GBs, which inhibits preferential oxidation of GBs and then enhances overall oxidation resistance of powder without sacrificing electrical conductivity. The enhanced oxidation resistance can be ascribed to high dissociation pressure of Ag_2O compared to Cu_2O and CuO ^{27,28}. This means that the preferential oxidation of GB could be inhibited by coverage of Ag phase. On the contrary, pure Cu particles suffer from a rapid oxidation throughout the oxidation process because of the poor oxidation resistance of GBs relative to that of grain interiors. This agrees well with the above results shown in Fig. 5.

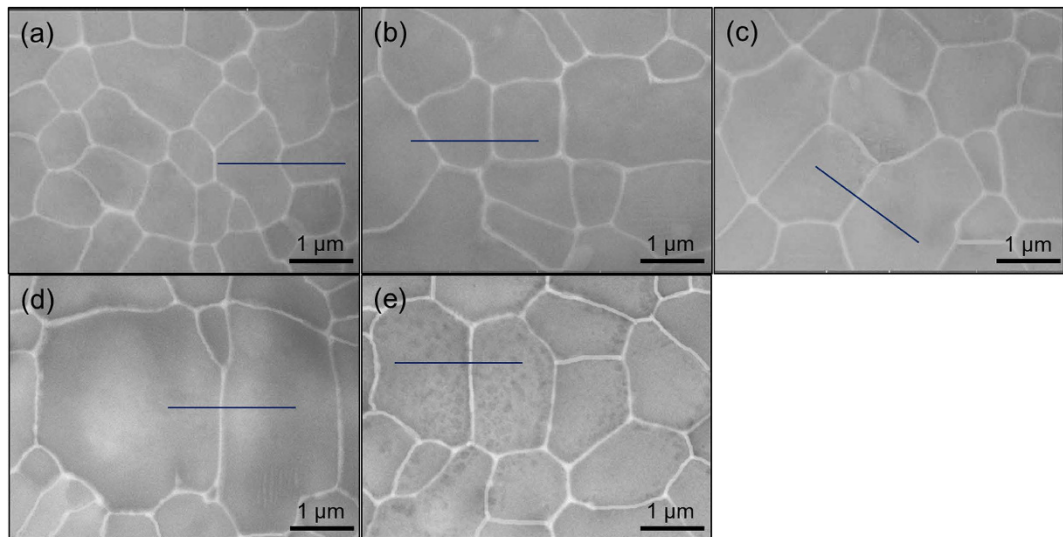


Figure 9. Structural evolution of the aged Cu-Ag powder. (a–e) Backscattered scanning electron images for the aged Cu-Ag powder after an oxidation period of 0 min (a), 1 min (b), 3 min (c), 5 min (d) and 10 min (e) at 200 °C.

The relationship between the mass change and oxidation temperature/time in our case can be expressed by²⁹:

$$y^3 = 3k_0 t e^{-\frac{Q}{RT}} \quad (1)$$

where y is mass change ($\Delta m/m_0$) at time t ; k_0 is the temperature-independent pre-exponential; Q is the energy of activation; T is the absolute temperature; and R is the universal gas constant. The dependence of oxidation rate on temperature can also be defined by the Arrhenius equation,

$$k_c = k_0 \exp\left(-\frac{Q}{RT}\right) \quad (2)$$

where k_c represents cubic rate constant (min^{-1}) at each temperature for three powders. Substituting k_c into Eq. (1) yields a linear expression,

$$y^3 = 3k_c t \quad (3)$$

Thus, the oxidation rate can be determined by Eq. (3). Table 1 lists the k_c values for the linear segment of curves together with the correlation coefficient value, r^2 . All the r^2 values approach 1, indicating that the cubic oxidation law is reasonably applicable to the oxidation behavior. By plotting k_c against reciprocal of temperature, the activation energy of oxidation can be generated from the slope of every fitting line, as shown in Fig. 11. The activation energies of the Cu and as-atomized Cu-Ag powders are calculated to be 83 and 114 kJ/mol, respectively. In contrast, the activation energy of the aged Cu-Ag powder is much higher (167 kJ/mol), implying that the aging-treated Cu-Ag powder undergoes a slow oxidation (Table 1).

The activation energies of oxidation, Q for the three powders are compared with those of bulk Cu—oxygen-free high-conductivity Cu (OFHC) (99.9999 pct (6N) Cu and 99.99 pct (4N) Cu), as listed in Table 2. A typical Q for the pure Cu has been reported to be in the range of 40–85 kJ/mol at 300–550 °C^{30–32}, and 158–173 kJ/mol at 800–1050 °C^{31,33}. Our present pure Cu powder oxidized at 200–350 °C also has a Q of 83 kJ/mol, which agrees with the previously reported value.

It is widely accepted that GB diffusion predominates during oxidation of Cu at low temperature (<550 °C), while at high temperature (>900 °C) lattice diffusion is dominated during oxidation^{33,34}. It is interesting to find that the aging-treated Cu-Ag at 200–350 °C demonstrates a Q value as high as that of pure Cu at high temperature, implying that the oxidation of aged Cu-Ag powder is possibly linked to the lattice diffusion of Cu, since the diffusion of Cu at GBs is blocked due to the continuous distribution of Ag phase. The Q of as-atomized Cu-Ag powder at 200–350 °C is close to that of 6N copper at intermediate temperatures of 600–850 °C, where the oxidation relies on both GB diffusion and lattice diffusion^{33,34}.

The successful use of inert and conducting Ag rich in GBs of a Cu-Ag powder represents a remarkable step forward in realizing high electrical conductivity and high oxidation resistance for a broad range of electrical transfer applications. Our results demonstrate, for the first time, that the unique resultant microstructure leads to the effective inhibition of oxidation of the Cu powder while not sacrificing the electrical conductivity. Such an outstanding combination of oxidation resistance and electrical conductivity in Cu-Ag powders holds substantial promise as a new material platform for further development of electrical transfer powder.

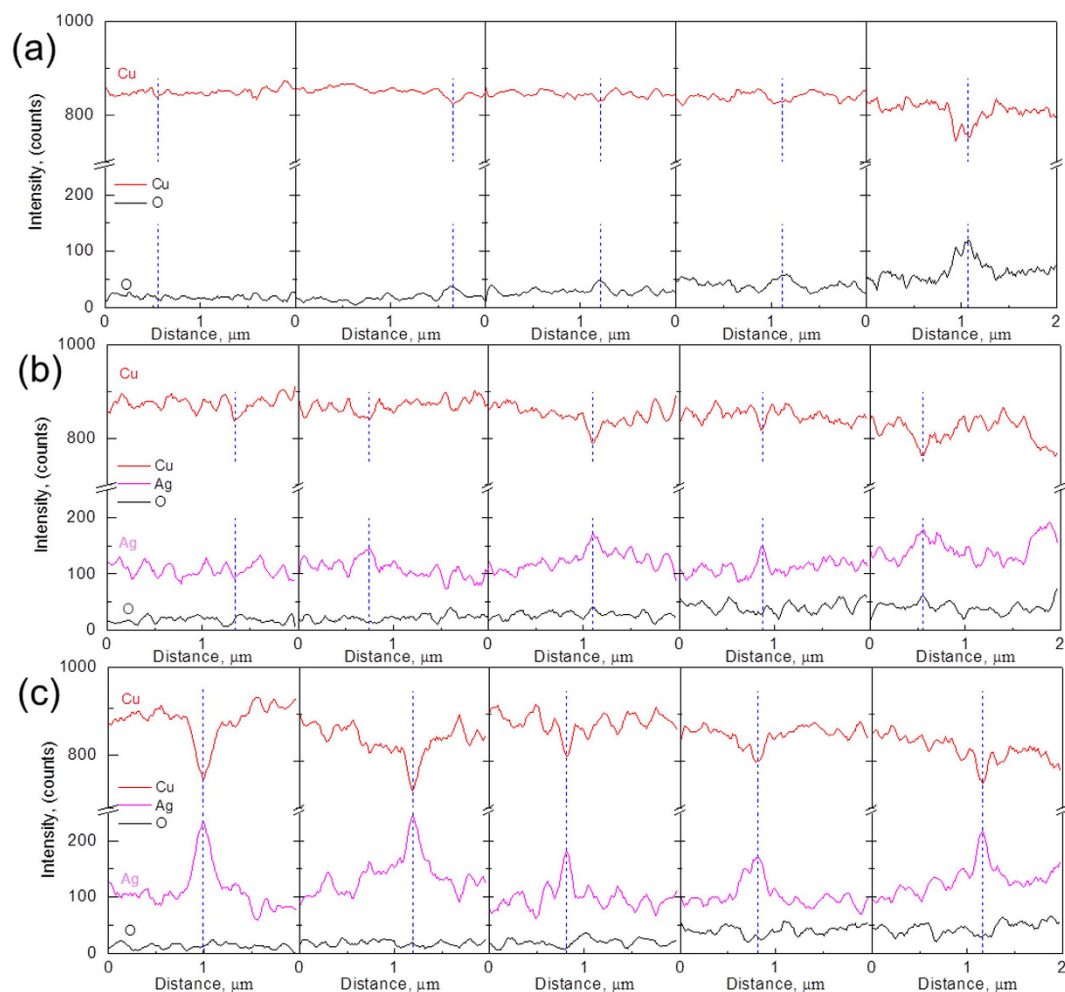


Figure 10. Line-scan analysis. (a–c) Line-scan profiles of the white lines (a) in Fig. 5(a–e), the crimson lines (b) in Fig. 6(a–e) and the dark blue lines (c) in Fig. 7(a–e).

Cubic constant $k_c / \text{min}^{-1}, (R^2)$	200 °C	250 °C	300 °C	350 °C	E_a , kJ/mol
Pure Cu powder	6.23×10^{-3} (0.99698)	1.34×10^{-2} (0.99658)	6.85×10^{-2} (0.99849)	3.47×10^{-1} (0.99992)	83.03 (0.99619)
Initial Cu–Ag powder	6.90×10^{-4} (0.99939)	5.40×10^{-3} (0.99947)	4.07×10^{-2} (0.99969)	2.58×10^{-1} (0.99542)	113.72 (0.99504)
Aged Cu–Ag powder	2.29×10^{-5} (0.99515)	6.90×10^{-4} (0.99691)	2.95×10^{-2} (0.99735)	1.98×10^{-1} (0.99798)	166.53 (0.99667)

Table 1. Cubic rate constant k_c , correlation coefficient R^2 , and activation energy E_a for the three types of powders.

Methods

Sample preparation. Two kinds of Cu-based powders, pure Cu (>99.8%) and Cu–5Ag (mass%) alloy, were applied as starting materials. The two powders were fabricated by a Hermiga gas atomizer (PSI, Hailsham, East Sussex, UK), which enabled us to obtain extremely low oxygen content (<0.0080 mass%, see in Table S1), good spherical shape (Fig. 1a,b) and comparable size distribution after sifting (Fig. S2). A graphite crucible containing ingots was placed into the atomizer, which was then heated to 1200 °C at a rate of 50 °C/min. High-purity argon gas ($\geq 99.99\%$) emitted at a constant pressure of 2.0 MPa and high-vacuum reactor (1.7 Pa) were used to ensure the low oxygen content. The as-atomized Cu–Ag alloy powder (5 g at each condition) was contained in an alumina crucible and placed into a tubular resistance furnace, being aged with a constant hydrogen flow rate of 500 ml/min at 100 °C, 125 °C, 150 °C, 200 °C and 250 °C for the duration of 5, 10, 30, 60, 90 and 120 min, respectively. One end of the furnace was equipped with a H_2 inlet and at the other end H_2 was ignited in air. Before H_2 flowing into the tubular furnace, N_2 was flowed for 5 min to get rid of O_2 . To probe oxidation process of the powders, we conducted TGA analyses in dry air using a SDT Q600 analyzer (TA Instruments, USA) under a heating rate of 30 °C/min from room temperature to 400 °C. The isothermal oxidation test was carried out at 200, 250, 300 and 350 °C for

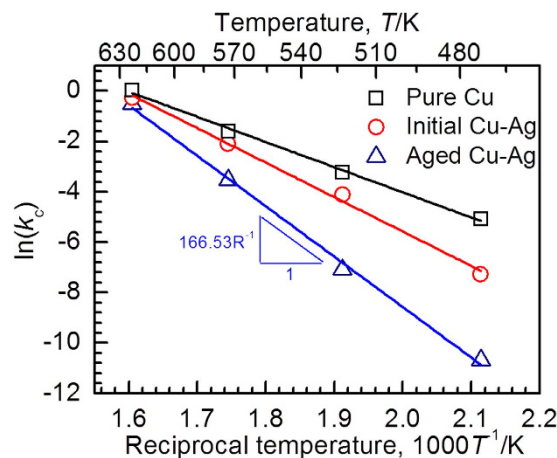


Figure 11. Arrhenius plot. Arrhenius plot of cubic rate constants during the oxidation process for the three different types of powders at air.

Starting material	Atmospheric condition (1 atm)	Temperature range (°C)	Activation energy (kJ/mol)	Ref.
OFHC (99.9%)	O ₂	300–550	84	Valensi ³¹
		500–900	158	
99.90%	Air	250–500	71	O'reilly ³²
99.99%	O ₂	350–550	52	Zhu ³³
		600–900	95	
		900–1050	173	
100.00%	O ₂	350–550	40	Zhu ³³
		600–850	111	
		850–1050	173	
Pure Cu powder	Air	200–350	83	Present work
Initial Cu-Ag powder	Air	200–350	114	
Aged Cu-Ag powder	Air	200–350	167	

Table 2. Activation energies for the different Cu-related materials.

up to 3 h. The electrical conductivity of the powders was measured by using FT-300 powder conductivity tester (Rooko Instrument Co., China).

Structural characterization. To characterize microstructure of the particles from the cross-section direction, the powders were first cold-mounted in epoxy, followed by grinding with 1000 and 2000-mesh SiC abrasive paper and polishing in OP-S solution for 30 min. Microstructural observation from both the cross section and surface of the particles was conducted using scanning electron microscopy (SEM; S-3400N, Hitachi, Tokyo, Japan) equipped with energy-dispersive spectroscopy (EDS) and an electron probe micro-analyzer (EPMA). The particle size of 10–30 μm was chosen for the observation.

References

- Li, Y. & Wong, C. P. Recent advances of conductive adhesives as a lead-free alternative in electronic packaging: Materials, processing, reliability and applications. *Mater. Sci. Eng. R: Rep.* **51**, 1–35 (2006).
- Yang, C., Wong, C. & Yuen, M. M. F. Printed electrically conductive composites: conductive filler designs and surface engineering. *J. Mater. Chem. C* **1**, 4052–4069 (2013).
- Chung, D. D. L. Electromagnetic interference shielding effectiveness of carbon materials. *Carbon* **39**, 279–285 (2001).
- Li, Y., Wu, Y. & Ong, B. S. Facile Synthesis of Silver Nanoparticles Useful for Fabrication of High-Conductivity Elements for Printed Electronics. *J. Am. Chem. Soc.* **127**, 3266–3267 (2005).
- Wu, S. Preparation of fine copper powder using ascorbic acid as reducing agent and its application in MLCC. *Mater. Lett.* **61**, 1125–1129 (2007).
- Krumbein, S. J. Metallic electromigration phenomena. *IEEE Transactions on Components, Hybrids, and Manufacturing Technology* **11**, 5–15 (1988).
- Yang, S., Wu, J. & Christou, A. Initial stage of silver electrochemical migration degradation. *Microelectronics Reliability* **46**, 1915–1921 (2006).
- Li, J., Mayer, J. W. & Colgan, E. G. Oxidation and protection in copper and copper alloy thin films. *J. Appl. Phys.* **70**, 2820–2827 (1991).
- Ogbuji, L. & Humphrey, D. L. Comparison of the oxidation rates of some new copper alloys. *Oxidation of Metals* **60**, 271–291 (2003).

10. Ding, P. J., Lanford, W. A., Hymes, S. & Murarka, S. P. Effects of the addition of small amounts of Al to copper: corrosion, resistivity, adhesion, morphology, and diffusion. *J. Appl. Phys.* **75**, 3627–3631 (1994).
11. Ding, P. J., Lanford, W. A., Hymes, S. & Murarka, S. P. Oxidation resistant high conductivity copper films. *Appl. Phys. Lett.* **64**, 2897–2899 (1994).
12. Mondolfo, L. F. *Aluminum Alloys: Structure and Properties*. (Elsevier, 2013).
13. Grouchko, M., Kamyshny, A. & Magdassi, S. Formation of air-stable copper-silver core-shell nanoparticles for inkjet printing. *J. Mater. Chem.* **19**, 3057–3062 (2009).
14. Peng, Y. H. *et al.* Study on synthesis of ultrafine Cu-Ag core-shell powders with high electrical conductivity. *Appl. Surf. Sci.* **263**, 38–44 (2012).
15. Kim, C. K., Lee, G. J., Lee, M. K. & Rhee, C. K. A novel method to prepare Cu@Ag core-shell nanoparticles for printed flexible electronics. *Powder Technology* **263**, 1–6 (2014).
16. Tsai, C. H., Chen, S. Y., Song, J. M., Chen, I. G. & Lee, H. Y. Thermal stability of Cu@Ag core-shell nanoparticles. *Corros. Sci.* **74**, 123–129 (2013).
17. Hai, H. T., Takamura, H. & Koike, J. Oxidation behavior of Cu-Ag core-shell particles for solar cell applications. *J. Alloys Compd.* **564**, 71–77 (2013).
18. Ul-Hamid, A. A microstructural study of preferential oxidation at the grain boundaries of Ni-Cr alloys. *Oxidation of Metals* **57**, 217–230 (2002).
19. Callister, W. D. *Fundamentals of Materials Science and Engineering*. 5th edn, 115–117 (Wiley, 2011).
20. Divinski, S., Lohmann, M. & Herzig, C. Ag grain boundary diffusion and segregation in Cu: measurements in the types B and C diffusion regimes. *Acta Mater.* **49**, 249–261 (2001).
21. Benghalem, A. & Morris, D. G. Microstructure and strength of wire-drawn Cu-Ag filamentary composites. *Acta Mater.* **45**, 397–406 (1997).
22. Sakai, Y., Inoue, K., Asano, T., Wada, H. & Maeda, H. Development of high-strength, high-conductivity Cu-Ag alloys for high-field pulsed magnet use. *Appl. Phys. Lett.* **59**, 2965–2967 (1991).
23. Sakai, Y. & Schneider-Muntau, H. J. Ultra-high strength, high conductivity Cu-Ag alloy wires. *Acta Mater.* **45**, 1017–1023 (1997).
24. Niu, Y., Huntz, A. M., Gesmundo, F. & Castello, P. The air oxidation of a Cu-5 wt% Ag alloy at 650–750 °C. *Materials Science Forum* **251–254**, 73–80 (1997).
25. Gesmundo, F. *et al.* The sulfidation of two-phase Cu-Ag alloys in H₂-H₂S mixtures at 550–750 °C. *Corros. Sci.* **38**, 1295–1317 (1996).
26. Li, J., Zhuang, Y. & Lin, W. The ternary system Ag-Cu-Ho at 500 °C. *J. Alloys Compd.* **191**, 187–189 (1993).
27. Gaskell, D. R. *et al.* *Introduction to the Thermodynamics of Materials*. 5th edn, 59 (Taylor & Francis, 2008).
28. Chang, Y. A. & Oates, W. A. *Materials Thermodynamics*. 279 (Wiley, 2010).
29. Rhodin, T. N. Jr. Low temperature oxidation of copper. I. physical mechanism^{1a}. *J. Am. Chem. Soc.* **72**, 5102–5106 (1950).
30. Vernon, W. H. J. The formation of protective oxide films on copper and brass by exposure to air at various temperatures. *J. Am. Chem. Soc.* **129**, 2273–2282 (1926).
31. Valensi, G. Theoretical and experimental investigations about conjugated formation of several layers, in International Conference on Surface Reactions, Pittsburgh, Corrosion Publ. Co., 156–164 (1948).
32. O'Reilly, M. *et al.* Investigation of the oxidation behaviour of thin film and bulk copper. *Appl. Surf. Sci.* **91**, 152–156 (1995).
33. Zhu, Y., Mimura, K., Lim, J. W., Isshiki, M. & Jiang, Q. Brief review of oxidation kinetics of copper at 350 °C to 1050 °C. *Metall. Mater. Trans. A* **37**, 1231–1237 (2006).
34. Gonçalves, A. M. B., Campos, L. C., Ferlauto, A. S. & Lacerda, R. G. On the growth and electrical characterization of CuO nanowires by thermal oxidation. *J. Appl. Phys.* **106**, (2009).

Acknowledgements

The authors gratefully acknowledge the financial support from project of The Science Fund for Distinguished Young Scholars of Hunan Province, China (2016JJ1016), Fund of State Key Lab for Powder Metallurgy, Central South University. Z.W. acknowledges financial support from the National Natural Science Foundation of China (Grant no. 11332013).

Author Contributions

Y. Li designed the idea; J. Li, G. Xu, Y. Li, Y. Hou, and H. Bian designed the experiments. Y. Hou, H. Bian and F. Wang performed the EPMA experiments; J. Li performed all the rest experiments and analyzed the data. Z. Wang and Y. Li prepared the manuscript; Z. Wang revised the grammar; all authors reviewed the manuscript.

Additional Information

Supplementary information accompanies this paper at <http://www.nature.com/srep>

Competing financial interests: The authors declare no competing financial interests.

How to cite this article: Li, J. *et al.* Ultrahigh Oxidation Resistance and High Electrical Conductivity in Copper-Silver Powder. *Sci. Rep.* **6**, 39650; doi: 10.1038/srep39650 (2016).

Publisher's note: Springer Nature remains neutral with regard to jurisdictional claims in published maps and institutional affiliations.



This work is licensed under a Creative Commons Attribution 4.0 International License. The images or other third party material in this article are included in the article's Creative Commons license, unless indicated otherwise in the credit line; if the material is not included under the Creative Commons license, users will need to obtain permission from the license holder to reproduce the material. To view a copy of this license, visit <http://creativecommons.org/licenses/by/4.0/>

© The Author(s) 2016